Eur. Phys. J. Plus (2018) **133**: 360
DOI 10.1140/epjp/i2018-12167-x

THE EUROPEAN PHYSICAL JOURNAL PLUS

Regular Article

Electron acoustic waves in a 2-electron, dissipative, quantum magneto plasma

Biswajit Sahu[1,a], Anjana Sinha[2,b], and Rajkumar Roychoudhury[3,4,c]

[1] Department of Mathematics, West Bengal State University, Barasat, Kolkata - 700126, India
[2] Physics and Applied Mathematics Unit, Indian Statistical Institute, Kolkata - 700108, India
[3] Department of Mathematics, Bethune College, 181 Bidhan Sarani, Kolkata - 700006, India
[4] Department of Mathematics Education, Visva Bharati, Santiniketan 731204, India

Received: 3 May 2018 / Revised: 9 July 2018
Published online: 11 September 2018

Abstract. A theoretical study is presented for the oblique propagation of linear and nonlinear electron acoustic waves (EAWs) in a two-electron population, dissipative, quantum magnetoplasma. The linear dispersion relation yields a complex plasma wave frequency ω, denoting a decaying wave, with the amount of damping directly related to the strength of the dissipative force. The small amplitude analysis for the nonlinear structures using the reductive perturbation technique, gives the Korteweg-de Vries-Burgers equation. The numerical solutions depict a soliton for negligible dissipation and a monotonic shock for relatively large dissipation. For intermediate values, the solutions are damped oscillations. The dispersion of the EAWs gets enhanced with increase in strength of the magnetic field and a higher value of the ratio of hot to cold electron density. The stability analysis is also carried out, and the corresponding phase portraits are plotted to observe the trajectories. Of the two critical points, one is a saddle point, hence always unstable, while the other is a stable focus or a stable node, depending on the relative strengths of the plasma parameters.

1 Introduction

Electron acoustic waves (EAWs), initially conceived by Fried and Gould way back in 1961 [1], are studied widely because of their potential importance in a variety of phenomena, from naturally occurring space plasmas [2–4], geomagnetic tail [5,6], to those artificially created in the laboratory [7–9]. These nonlinear waves exist in a two-temperature (hot and cold) electron plasma, or electron-ion plasma with the ions hotter than the electrons [10]. For the generation of such EAWs in a non-thermal plasma consisting of two species of electrons at two different temperatures, against a stationary background of neutralizing ions, the required inertia is provided by the cold electrons whereas the restoring force is obtained from the thermal pressure provided by the inertialess hot electrons [11]. Typically, the frequency of these waves is much higher as compared to the ion plasma frequency. The easier mobility of the cold electrons as compared to the heavier ions ensures stronger Landau damping of EAWs than ion-acoustic waves [12]. The hot electrons being inertialess, the dynamics of the EAWs is primarily related to the dynamics of the cold electrons.

Most studies on EAWs are in classical plasma [13–25]. However, quantum effects become significant at very high densities like laser produced plasmas [26–29] and in dense astrophysical environments [30–33]. In the present work, we shall study nonlinear wave propagation in a two-electron population dense quantum plasma, in the presence of an external magnetic field, and a dissipative force. Since these waves exist at moderately small amplitudes [13], we shall restrict ourselves to small amplitude analysis in this article. It is worth mentioning here that propagation of IAWs (ion acoustic waves) in degenerate relativistic quantum plasma with heavy nuclei, was taken up in ref. [34] whereas EAWs propagation was studied in a magnetised quantum plasma in ref. [11], but without any dissipation. So our emphasis in the present study shall be on this additional term.

[a] e-mail: biswajit_sahu@yahoo.co.in
[b] e-mail: sinha.anjana@gmail.com
[c] e-mail: rroychoudhury123@gmail.com

The organization of the work is as follows: in sect. 2 we introduce the basic governing equations and carry out the linear analysis in sect. 3. To study the small amplitude weak dissipative waves, we apply the reductive perturbation theory in sect. 4 and arrive at the dissipative Korteweg-de Vries-Burgers (KdVB) equation. We perform the stability analysis and verify our observations by drawing the corresponding trajectories in the phase plane. The numerical solutions are plotted using Mathematica. In fact, our focus is to see the effect of the different plasma parameters like dissipation, fractional density of hot to cold electrons and the magnetic field on the EAWs. Finally, we conclude our observations in sect. 5.

2 Nonlinear governing equations

The subject of our study is a dense magnetoplasma, consisting of hot electrons, cold electrons and stationary ions in the background [11]. Now, in a quantum plasma, the Fermi temperature T_{Fj} is directly related to the electron concentration n_j through the formula $T_{Fj} = (3\pi^2 n_j)^{2/3}\hbar^2/2mk_B$, where $j = h, c$ denotes hot and cold electrons respectively, n_j is the total number density, k_B is the Boltzman constant, and m is the electron mass. So, basically, *hot* and *cold* electrons refer to *thickly* and *sparsely populated* electrons, respectively. Our assumptions in this work are $n_c \ll n_h \Rightarrow T_{Fc} \ll T_{Fh}$. So the Fermi pressure due to cold electrons could be ignored in comparison with the hot electrons [35]. To avoid Landau damping, the phase speed of EAWs is assumed to be large as compared to the cold electron Fermi velocity, but small as compared to the Fermi velocity of hot electrons: $v_{Fc} \ll \omega/k \ll v_{Fh}$, where the Fermi speed $v_{Fj} = \sqrt{2k_B T_{Fj}/m}$. Furthermore, we assume the external magnetic field to be pointed in the z direction: $\vec{B} = B_0\hat{z}$, and propagation to be in the x-z plane. If n_{j0} represents the equilibrium value of the total number density of the i-th species, then charge neutrality condition at equilibrium implies $n_{h0} + n_{c0} = Z_i n_{i0}$, i standing for ion. Now, in 3 dimensions, the hot electron pressure is given by

$$P_h = \frac{1}{5} m v_{Fh}^2 n_{h0} \left(\frac{n_h}{n_{h0}}\right)^{5/3}. \tag{1}$$

We shall study the dynamics of electron acoustic waves (EAWs) in the low-frequency limit: $\omega \ll \omega_{cc}$ where the electron Larmor frequency $\omega_{cc} = \frac{eB_0}{mc}$. The basic governing equations for such a plasma in the presence of cold electron kinematic viscosity μ, in the framework of quantum magneto hydrodynamic (QMHD) model are given as [36,37]

$$\frac{\partial n_c}{\partial t} + \vec{\nabla}\cdot(n_c\vec{u}_c) = 0, \tag{2}$$

$$\frac{\partial \vec{u}_c}{\partial t} + \left(\vec{u}_c\cdot\vec{\nabla}\right)\vec{u}_c = \frac{e}{m}\vec{\nabla}\Phi - \frac{e}{mc}\left(\vec{u}_c\times\vec{B}\right) + \frac{\hbar^2}{2m^2}\vec{\nabla}\left(\frac{1}{\sqrt{n_c}}\right)\nabla^2\sqrt{n_c} + \frac{\mu}{mn_c}\nabla^2\vec{u}_c, \tag{3}$$

$$\frac{e}{m}\vec{\nabla}\Phi - \frac{1}{mn_h}\vec{\nabla}P_h + \frac{\hbar^2}{2m^2}\vec{\nabla}\left(\frac{1}{\sqrt{n_h}}\right)\nabla^2\sqrt{n_h} = 0, \tag{4}$$

$$\nabla^2\Phi = 4\pi e\left(n_c + n_h - Z_i n_i\right). \tag{5}$$

Next we apply the following normalizations:

$$\bar{r} = \frac{\omega_{pc}}{c_{se}}r, \qquad \bar{t} = \omega_{pc}t, \qquad \bar{n}_j = \frac{n_j}{n_{j0}}, \qquad \bar{u}_j = \frac{u_j}{c_{se}}, \qquad \bar{\Phi} = \frac{\Phi}{\Phi_0}, \qquad \bar{\omega}_{cc} = \frac{\omega_{cc}}{\omega_{pc}}, \qquad \bar{P}_h = \frac{P_h}{2k_B T_{Fh} n_{h0}}, \tag{6}$$

where $\Phi_0 = 2k_B T_{Fh}/e$, the ratio of background hot to cold electron number densities is denoted as $\alpha = n_{h0}/n_{c0}$, and the quantum electron acoustic speed and the cold electron plasma speed ω_{pc} are respectively given by

$$\omega_{pc} = \sqrt{\frac{4\pi n_{c0}e^2}{m}}, \qquad c_{se} = \sqrt{\frac{2k_B T_{Fh}}{m\alpha}}. \tag{7}$$

Now, $n_{h0} \gg n_{c0}$ implies $\omega_{pc}^{-1} \gg \omega_{ph}^{-1}$; *i.e.*, the oscillation time scale of the cold electrons ($\sim \omega_{pc}^{-1}$) is much greater than that of the hot electrons ($\sim \omega_{ph}^{-1}$). In this slow time scale, the hot electrons move fast enough to maintain thermodynamic equilibrium.

Defining the non-dimensional quantum parameter H as

$$H = \frac{\hbar\omega_{pc}}{mc_{se}^2} = \frac{\hbar e\alpha}{k_B T_F}\sqrt{\frac{\pi n_{c0}}{m}}, \tag{8}$$

it is easy to observe that H is directly proportional to α.

Dropping the bars for simplicity of notation, the basic set of normalized governing equations in the framework of QMHD model, for a dissipative 2-electron quantum plasma, in the presence of a magnetic field may be written as

$$\frac{\partial n_c}{\partial t} + \vec{\nabla} \cdot (n_c \vec{u}_c) = 0, \tag{9}$$

$$\frac{\partial \vec{u}_c}{\partial t} + \left(\vec{u}_c \cdot \vec{\nabla}\right) \vec{u}_c = \alpha \vec{\nabla}\phi - \omega_{cc} \left(\vec{u}_c \times \hat{z}\right) + \frac{H^2}{2} \vec{\nabla} \left(\frac{1}{\sqrt{n_c}}\right) \nabla^2 \sqrt{n_c} + \eta \nabla^2 \vec{u}_c, \tag{10}$$

$$\vec{\nabla}\Phi - \frac{1}{3} n_h^{-1/3} \vec{\nabla} n_h + \frac{H^2}{2} \vec{\nabla} \left(\frac{1}{\sqrt{n_h}}\right) \nabla^2 \sqrt{n_h} = 0, \tag{11}$$

$$\nabla^2 \Phi = \frac{1}{\alpha} n_c + n_h - \left(1 + \frac{1}{\alpha}\right), \tag{12}$$

where $\eta = \frac{\mu}{m n_c}$ is the cold electron dynamic viscosity, and $\bar{\eta} = \eta \frac{\omega_{pc}^2}{c_{se}^2}$ is its normalized value. In component form, the governing equations reduce to

$$\frac{\partial n_c}{\partial t} + \frac{\partial}{\partial x} (n_c u_{cx}) + \frac{\partial}{\partial z} (n_c u_{cz}) = 0, \tag{13}$$

$$\frac{\partial u_{cx}}{\partial t} + \left(u_{cx} \frac{\partial}{\partial x} + u_{cz} \frac{\partial}{\partial z}\right) u_{cx} = \alpha \frac{\partial \phi}{\partial x} - \omega_{cc} u_{cy} + \frac{H^2}{2} \frac{\partial}{\partial x} \left\{ \frac{1}{\sqrt{n_c}} \left(\frac{\partial^2}{\partial x^2} + \frac{\partial^2}{\partial z^2}\right) \sqrt{n_c} \right\} + \eta \left(\frac{\partial^2}{\partial x^2} + \frac{\partial^2}{\partial z^2}\right) u_{cx}, \tag{14}$$

$$\frac{\partial u_{cy}}{\partial t} + \left(u_{cx} \frac{\partial}{\partial x} + u_{cz} \frac{\partial}{\partial z}\right) u_{cy} = \omega_{cc} u_{cx}, \tag{15}$$

$$\frac{\partial u_{cz}}{\partial t} + \left(u_{cx} \frac{\partial}{\partial x} + u_{cz} \frac{\partial}{\partial z}\right) u_{cz} = \alpha \frac{\partial \Phi}{\partial z} - \omega_{cc} u_{cy} + \frac{H^2}{2} \frac{\partial}{\partial z} \left\{ \frac{1}{\sqrt{n_c}} \left(\frac{\partial^2}{\partial x^2} + \frac{\partial^2}{\partial z^2}\right) \sqrt{n_c} \right\} + \eta \left(\frac{\partial^2}{\partial x^2} + \frac{\partial^2}{\partial z^2}\right) u_{cz}, \tag{16}$$

$$\frac{\partial \Phi}{\partial x} - \frac{1}{3} n_h^{-1/3} \frac{\partial n_h}{\partial x} + \frac{H^2}{2} \frac{\partial}{\partial x} \left\{ \frac{1}{\sqrt{n_c}} \left(\frac{\partial^2}{\partial x^2} + \frac{\partial^2}{\partial z^2}\right) \sqrt{n_c} \right\} = 0, \tag{17}$$

$$\frac{\partial \Phi}{\partial z} - \frac{1}{3} n_h^{-1/3} \frac{\partial n_h}{\partial z} + \frac{H^2}{2} \frac{\partial}{\partial z} \left\{ \frac{1}{\sqrt{n_c}} \left(\frac{\partial^2}{\partial x^2} + \frac{\partial^2}{\partial z^2}\right) \sqrt{n_c} \right\} = 0, \tag{18}$$

$$\frac{\partial^2 \Phi}{\partial x^2} + \frac{\partial^2 \Phi}{\partial z^2} = \frac{1}{\alpha} n_c + n_h - \left(1 + \frac{1}{\alpha}\right). \tag{19}$$

The full set of seven equations —*viz.*, (13) to (19)— describes the system. Now, to solve this entire set of equations is a tedious task, if not an impossible one. So, to have an insight into the system behaviour, we shall adopt different approximation methods like linearization, stability analysis, reductive perturbation technique to see the small amplitude structures, etc. In this regard, a phase portrait is a powerful graphical tool in visualizing the behaviour of the solutions in the long run, without actually solving the set of differential equations. We shall elaborate on these approaches one by one.

3 Linear analysis

In order to deduce a linear dispersion relation for the plasma waves, we assume the following expansions:

$$n_{c,h} = 1 + n_{c,h}^{(1)}, \qquad \phi = 0 + \phi^{(1)}, \qquad u_{c,j} = 0 + u_{c,j}^{(1)} \qquad (j = x, y, z), \tag{20}$$

with the perturbations $n_{c,h}^{(1)}$, $\phi^{(1)}$ and $u_{c,j}^{(1)}$ proportional to $e^{i(kx - \omega t)}$. Here ω and k are the perpendicular components of wave frequency and wave vector, respectively. After plugging in eq. (20) into eqs. (13)–(19), and considering the fact that the perturbations are proportional to $e^{i(kx-\omega t)}$, one obtains a quartic equation in ω,

$$\omega^4 + i d_1 \omega^3 + d_2 \omega^2 + i d_3 \omega + d_4 = 0, \tag{21}$$

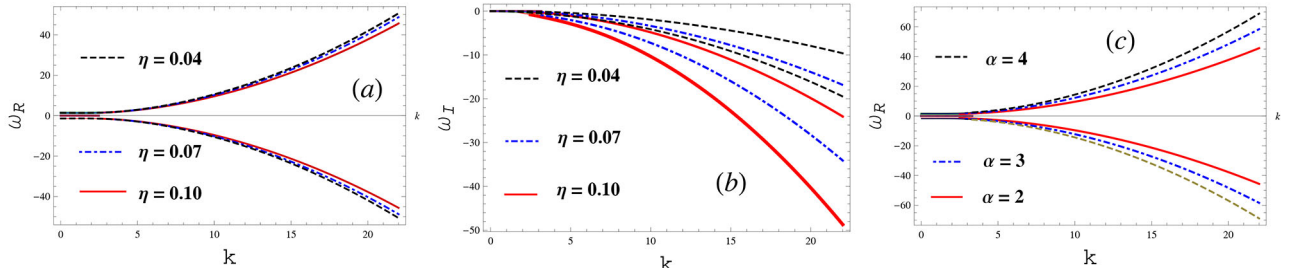

Fig. 1. (a) Plot of Re[ω] and (b) Plot of Im[ω], for different values of the dissipation parameter η, for $\alpha = 2$, $T_F = 1.5 \times 10^7\, K$, $B_0 = 3 \times 10^{10}\, G$, $n_{h0} = 1.1 \times 10^{26}\, \mathrm{cm}^{-3}$ and $l_z = 0.6$. (c) Plot of Re[ω] for different values of α, for $\eta = 0.1$, $T_F = 1.5 \times 10^7\, K$, $B_0 = 3 \times 10^{10}\, G$, $l_z = 0.4$.

where

$$d_1 = 2\eta k^2, \tag{22}$$

$$d_2 = -\left\{\eta^2 k^4 + \omega_{cc}^2 + \frac{H^2 k^4}{4} + \frac{\frac{1}{3} + \frac{H^2 k^4}{4}}{\sigma}\right\}, \tag{23}$$

$$d_3 = -\eta\left\{\omega_{cc}^2 k^2 + k^4\left(\frac{H^2 k^4}{4} + \frac{\frac{1}{3} + \frac{H^2 k^4}{4}}{\sigma}\right)\right\}, \tag{24}$$

$$d_4 = \omega_{cc}^2 k_z^2\left(\frac{H^2 k^4}{4} + \frac{\frac{1}{3} + \frac{H^2 k^4}{4}}{\sigma}\right), \tag{25}$$

with

$$\sigma = 1 + \frac{k^2}{3} + \frac{H^2 k^2}{4}. \tag{26}$$

In the absence of a dissipative term ($\eta = 0$), d_1, $d_3 = 0$, and we get back the result given in ref. [11].

We plot the real and imaginary parts of the wave frequency, ω_R and ω_I, respectively, in fig. 1, against the wavenumber k. Equation (21) has two real and two imaginary roots. The real part of the wave frequency (ω_R) is hardly affected by η, as seen in the left plot of fig. 1. The imaginary roots ω_I are negative, signifying damped or decaying wave. Increasing the dissipative term η, increases the magnitude of ω_I —thus the wave gets more and more damped, as seen in the middle plot of fig. 1. In the plot on the right, we show the variation of Re[ω] w.r.t. α. It is observed that the magnitude of ω_R increases with increase in α, *i.e.*, decrease in the number of cold electrons for a fixed number of hot electrons. Furthermore, it is observed that B_0 has a very little effect on ω_R, while ω_I remains unaffected by changes in α as well as B_0; hence these plots are not drawn here. As expected, ω_I is influenced by the dissipation term η only.

4 Small amplitude nonlinear structures

To investigate the propagation of electron-acoustic solitary waves in a magnetized quantum plasma, for weak dissipation, we adopt the standard reductive perturbation technique [38], stretching the independent variables as

$$\xi = \epsilon^{1/2}\left(l_x x + l_z z - Mt\right), \qquad \tau = \epsilon^{3/2} t, \tag{27}$$

where M is the Mach number, ϵ determines the strength of nonlinearity, and l_x, l_z are the direction cosines of the wave vector k along the x and z axes respectively, with $l_x^2 + l_z^2 = 1$. All physical quantities can be expanded in terms of power series in ϵ, about their equilibrium values as

$$\begin{aligned} n_{c,h} &= 1 + \epsilon n_{c,h}^{(1)} + \epsilon^2 n_{c,h}^{(2)} + \ldots, \\ \phi &= \epsilon\phi^{(1)} + \epsilon^2\phi^{(2)} + \ldots, \\ u_z &= \epsilon u_z^{(1)} + \epsilon^2 u_z^{(2)} + \epsilon^3 u_z^{(3)} + \ldots, \\ u_{x,y} &= \epsilon^{3/2} u_{x,y}^{(1)} + \epsilon^2 u_{x,y}^{(2)} + \epsilon^{5/2} u_{x,y}^{(3)} + \ldots. \end{aligned} \tag{28}$$

The strong magnetic field in the z direction introduces the anisotropy in the velocity components $u_{x,y,z}$. After plugging in eqs. (27) and (28) into eqs. (13)–(19), the first-order equations turn out to be

$$u_{cx}^{(1)}=0,\quad u_{cy}^{(1)}=\alpha\,\frac{l_x}{\omega_{cc}}\,\frac{\partial}{\partial\xi}\phi^{(1)},\quad u_{cz}^{(1)}=-\alpha\,\frac{l_z}{M}\phi^{(1)},\quad u_{cx}^{(2)}=-\alpha\,\frac{l_xM}{\omega_{cc}}\,\frac{\partial^2}{\partial\xi^2}\phi^{(1)},\quad u_{cy}^{(2)}=0,\quad n_c^{(1)}=-\alpha n_h^{(1)}=-3\alpha\phi^{(1)}, \tag{29}$$

whereas the second-order equations are obtained as

$$\begin{aligned}
&\frac{\partial^2}{\partial\xi^2}\phi^{(1)}=\frac{n_c^{(2)}}{\alpha}+n_h^{(2)},\\
&\frac{\partial n_c^{(1)}}{\partial\tau}-M\frac{\partial n_c^{(2)}}{\partial\xi}+2Mn_c^{(1)}\frac{\partial n_c^{(1)}}{\partial\xi}+\left(l_x\frac{\partial u_{cx}^{(2)}}{\partial\xi}+l_z\frac{\partial u_{cz}^{(2)}}{\partial\xi}\right)=0,\\
&\frac{\partial\phi^{(1)}}{\partial\tau}+\frac{M^2}{\alpha l_z}\frac{\partial u_{cz}^{(2)}}{\partial\xi}-\frac{\alpha l_z^2}{M}\phi^{(1)}\frac{\partial\phi^{(1)}}{\partial\xi}+M\frac{\partial\phi^{(2)}}{\partial\xi}+\frac{H^2}{4}\frac{M}{\alpha}\frac{\partial^3 n_c^{(1)}}{\partial\xi^3}-\eta_0\frac{\partial^2\phi^{(1)}}{\partial\xi^2}=0,\\
&\frac{\partial\phi^{(2)}}{\partial\xi}+\phi^{(1)}\frac{\partial\phi^{(1)}}{\partial\xi}+\frac{3}{4}H^2\frac{\partial^3\phi^{(1)}}{\partial\xi^3}-\frac{1}{3}\frac{\partial n_h^{(2)}}{\partial\xi}=0,
\end{aligned} \tag{30}$$

with $l_z=3M^2$. Since viscosity is a characteristic property of the medium, for weak values of this parameter, it can be stretched as $\eta=\eta_0\epsilon^{1/2}$ [13,39–41]. Mathematically, this is consistent with the nonlinear perturbation.

Equations (29) and (30) combined give the final equation as the Korteweg-de Vries-Burgers (KdVB) equation:

$$\frac{\partial n_c^{(1)}}{\partial\tau}+A_1n_c^{(1)}\frac{\partial n_c^{(1)}}{\partial\xi}+A_2\frac{\partial^3 n_c^{(1)}}{\partial\xi^3}+A_3\frac{\partial^2 n_c^{(1)}}{\partial\xi^2}=0, \tag{31}$$

where

$$\begin{aligned}
A_1&=M\left\{\frac{1}{2l_z}+\frac{1}{6\alpha}+\frac{1}{9\alpha^2}\right\},\\
A_2&=\frac{M}{2}\left\{\frac{1}{3}+\frac{1}{3\,\omega_{cc}}\left(1-l_z^2\right)-\frac{3}{2}H^2\right\},\\
A_3&=-\frac{1}{2}\eta_0,
\end{aligned} \tag{32}$$

with the quantum term H proportional to α, as defined in eq. (8). Thus A_1 is the nonlinearity coefficient, A_2 signifies dispersion and A_3 denotes dissipation. Evidently, for small amplitude waves, η is solely responsible for the dissipation in the system, while the external magnetic field determines the dispersion. The quantum effects also contribute to the dispersion of the nonlinear waves. In the absence of any dissipative force, eq. (31) reduces to the well known Korteweg-de Vries (KdV) equation with soliton solution, whereas for strong dissipation A_3 dominates over A_2, giving the Burgers equation with shock solution. Decreasing α increases the cold electron concentration of the ensemble, thus increasing the nonlinearity coefficient A_1. We shall now look into the stability of eq. (31) and plot its solutions numerically, using Mathematica.

4.1 Stability analysis

To examine the stationary solutions of eq. (31), we introduce a new variable

$$\zeta=\xi-U\tau, \tag{33}$$

where U is a constant velocity. To obtain the travelling wave solution to eq. (31), we transform it into the stationary wave frame

$$\frac{\partial^3 n_c^{(1)}}{\mathrm{d}\zeta^3}=\frac{U}{A_2}\,\frac{\mathrm{d}n_c^{(1)}}{\mathrm{d}\zeta}-\frac{A_1}{A_2}\,n_c^{(1)}\frac{\mathrm{d}n_c^{(1)}}{\mathrm{d}\zeta}-\frac{A_3}{A_2}\,\frac{\mathrm{d}^2n_c^{(1)}}{\mathrm{d}\zeta^2} \tag{34}$$

Now we integrate eq. (34) w.r.t. ζ once, subject to the boundary condition $n_c^{(1)}\to 1$ and $\mathrm{d}n_c^{(1)}/\mathrm{d}\zeta\to 0$, as $\zeta\to\infty$, to obtain

$$\frac{\partial^2 n_c^{(1)}}{\mathrm{d}\zeta^2}=\frac{U}{A_2}\,n_c^{(1)}-\frac{A_1}{A_2}\,\frac{n_c^{(1)\,2}}{2}-\frac{A_3}{A_2}\,\frac{\mathrm{d}n_c^{(1)}}{\mathrm{d}\zeta}+\frac{1}{A_2}\left(\frac{A_1}{2}-U\right). \tag{35}$$

Now, the above second-order equation (35) can be written as a system of two first-order equations as

$$\frac{\mathrm{d}n_c^{(1)}}{\mathrm{d}\zeta} = \bar{n} = P\left(n_c^{(1)}, \bar{n}\right) \text{ (say)}$$
$$\frac{\mathrm{d}\bar{n}}{\mathrm{d}\zeta} = -\frac{A_1}{2A_2}\, n_c^{(1)\,2} + \frac{U}{A_2}\, n_c^{(1)} - \left(\frac{U}{A_2} - \frac{A_1}{2A_2}\right) - \frac{A_3}{A_2}\,\bar{n} = Q\left(n_c^{(1)}, \bar{n}\right) \text{ (say)}. \tag{36}$$

In the $(n_c^{(1)}, \bar{n})$ plane, the set of eqs. (36) has two critical points. In this particular case, the roots of the corresponding linearized system turn out to be $(1, 0)$ and $(\frac{2U}{A_1} - 1, 0)$. For stability analysis, we have to solve the eigenvalue equation $|J - \lambda I| = 0$, where I is the identity matrix and the Jacobian J, given by

$$J = \begin{pmatrix} \dfrac{\partial P}{\partial n_c^{(1)}} & \dfrac{\partial P}{\partial \bar{n}} \\[2ex] \dfrac{\partial Q}{\partial n_c^{(1)}} & \dfrac{\partial Q}{\partial \bar{n}} \end{pmatrix}, \tag{37}$$

is evaluated at the critical points. The roots (say, λ_1, λ_2) of the eigenvalue equation determine the stability of the system [42]. If λ_1, λ_2 are real and distinct, the critical point is a *node* —if both are positive, the node is unstable, whereas if both are negative the node is stable. If λ_1, λ_2 are of opposite sign, the critical point is called a *saddle* point; it is always unstable. On the other hand, complex eigenvalues denote a *spiral* point —unstable *focus* if the real part is positive, and stable *focus* if the real part is negative. We shall check the stability at the critical points for physically relevant values of the parameters, remembering that A_3 is negative. In dense astrophysical environment, typical values of the plasma parameters are: magnetic field $B_0 \sim 10^{10}\,G$ to $10^{11}\,G$, Fermi temperature $T_f \sim 10^8\,K$ to $10^{10}\,K$ and $n_{h0} \sim 10^{29}\,\mathrm{cm}^{-3}$ to $10^{31}\,\mathrm{cm}^{-3}$ [11,43]. For $n_{c0} \ll n_{h0}$, we observe that $A_2 < 0$, so that

- at the critical point $(1, 0)$, $\lambda = -\frac{A_3}{A_2} \pm \frac{1}{A_2}\sqrt{A_3^2 + 4(U - A_1)A_2}$.

  Thus, the point $(1, 0)$ is a saddle point; hence always unstable
- at the critical point $(\frac{2U}{A_1} - 1, 0)$, $\lambda = -\frac{A_3}{A_2} \pm \frac{1}{A_2}\sqrt{A_3^2 - 4(U - A_1)A_2}$.

  Hence, for $A_3^2 > 4(U - A_1)A_2$, the point $(\frac{2U}{A_1} - 1, 0)$ is a stable node, and the shock wave has a monotonic profile, whereas for $A_3^2 < 4(U - A_1)A_2$, the point $(\frac{2U}{A_1} - 1, 0)$ is a stable focus, and the shock wave has an oscillatory profile.

We shall endorse our stability analysis with phase portrait diagrams and numerical plots in the next section.

4.2 Numerical plots

Now, as stated earlier, the dynamics of EAWs is mainly related to the dynamics of the cold electrons. So we shall study the influence of the dissipative force η, the external magnetic field B, and the hot to cold electron ratio α, on the leading-order cold electron density $n_c^{(1)}$, when EAWs propagate in a dissipative, quantum magnetoplasma. For this purpose, we find the numerical solution to eq. (31) using Mathematica, under boundary conditions $n_c^{(1)} \to 1$ and $\mathrm{d}n_c^{(1)}/\mathrm{d}\xi \to 0$ as $\xi \to \pm\infty$. We plot the cold electron concentration $n_c^{(1)}$ against ξ —for various values of η, α and B in fig. 2, fig. 4 and fig. 6, respectively. In the absence of any dissipative force (*i.e.*, for negligible values of η), we have a soliton solution as shown in fig. 2(a). This is expected as the KdVB eq. (31) reduces to the KdV equation. As η is increased, the waves get more and more damped —fig. 2(b) and 2(c). Finally, at some critical value of η, the Burgers term predominates and we get a monotonic shock solution as observed in fig. 2(d). The corresponding phase portraits are plotted in fig. 3. The blue dashed curve denotes the soliton solution of fig. 2(a). The oscillatory plot in fig. 2(b) corresponds to the solid magenta spiral in fig. 3. The very damped plot of fig. 2(c) is shown by the black dot-dashed curve in fig. 3. Finally the red saddle in fig. 3 corresponds to the monotonic shock solution in fig. 2(d). Additionally, the phase portraits drawn in fig. 3 indicate that the amplitude of the nonlinear structures decreases with increasing dissipation. Furthermore, it is evident from fig. 3 that the critical point $(1, 0)$ is an unstable saddle, whereas the other critical point $(\frac{2U}{A_1} - 1, 0)$ is asymptotically stable. Thus the trajectories plotted in fig. 3 validate the stability analysis.

The hot to cold electron ratio at equilibrium has just the opposite effect on the shape of the nonlinear structures. As α decreases, *i.e.*, the relative number density of cold electrons increases, the oscillatory solution gets more and more damped, along with decrease in dispersion —fig. 4. Figure 5 shows the corresponding phase portraits. The solid

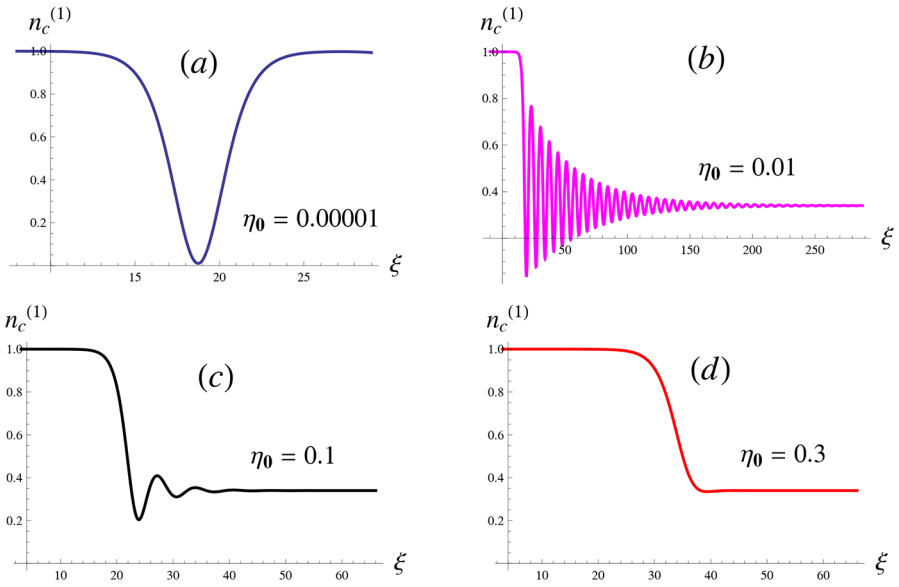

Fig. 2. Plot of $n_c^{(1)}$ for different values of η_0, for $\alpha = 5$, $T_F = 1.5 \times 10^8\, K$, $B_0 = 5 \times 10^{10}\, G$, $n_{h0} = 1.1 \times 10^{29}\, \mathrm{cm}^{-3}$ and $l_z = 0.8$.

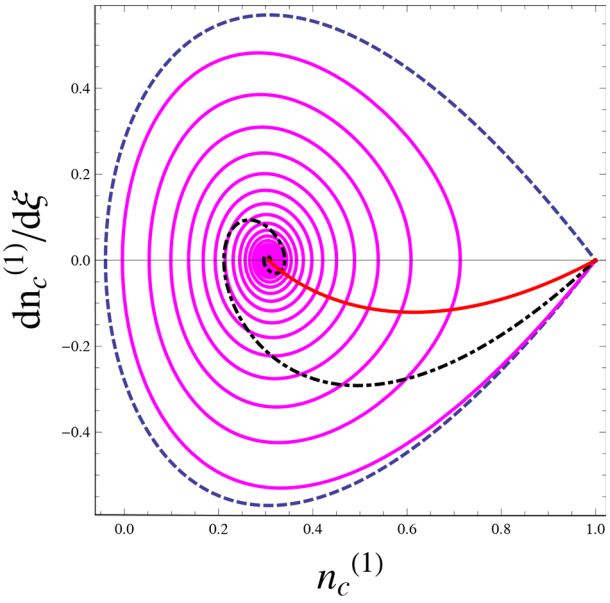

Fig. 3. Plot showing phase portraits $n_c^{(1)}$ *versus* $\mathrm{d}n_c^{(1)}/\mathrm{d}\xi$ for different values of η_0, for $\alpha = 5$, $T_F = 1.5 \times 10^8\, K$, $B_0 = 5 \times 10^{10}\, G$, $n_{h0} = 1.1 \times 10^{29}\, \mathrm{cm}^{-3}$ and $l_z = 0.8$.

blue trajectory in fig. 5 is for the lowest value of α, whereas the magenta trajectory is for the highest α value. The decrease in the amplitude as well as width of the waves with increase in α is quite evident. The stability analysis at the two critical points is also verified. Now, from eq. (8), the quantum term H is proportional to α. So, the quantum term H has a similar impact on the nonlinear electron acoustic waves, as that of α.

As observed from the coefficients in eq. (31), the magnetic field B_0 is present in the dispersion coefficient A_2 only, through the term ω_{cc}. When we plot the numerical solutions for varying B_0 in fig. 6, we observe that as the magnetic field is increased, the dispersion gets enhanced and the oscillations increase, without any change in amplitude. A relatively weaker magnetic field may not support an oscillatory wave, giving a monotonic shock —fig. 6(a). The corresponding trajectories in the phase plane are plotted in fig. 7 —the black dotted saddle for the lowest value of B_0 and the red dot dashed spiral for its highest value. These plots authenticate the following observations:

– the amplitude of the nonlinear waves is not affected by the magnitude of the external magnetic field;
– a stronger magnetic field enhances dispersion;
– oscillations prevail for a longer time with increase in B_0;
– the stability analysis at the 2 critical points is authenticated.

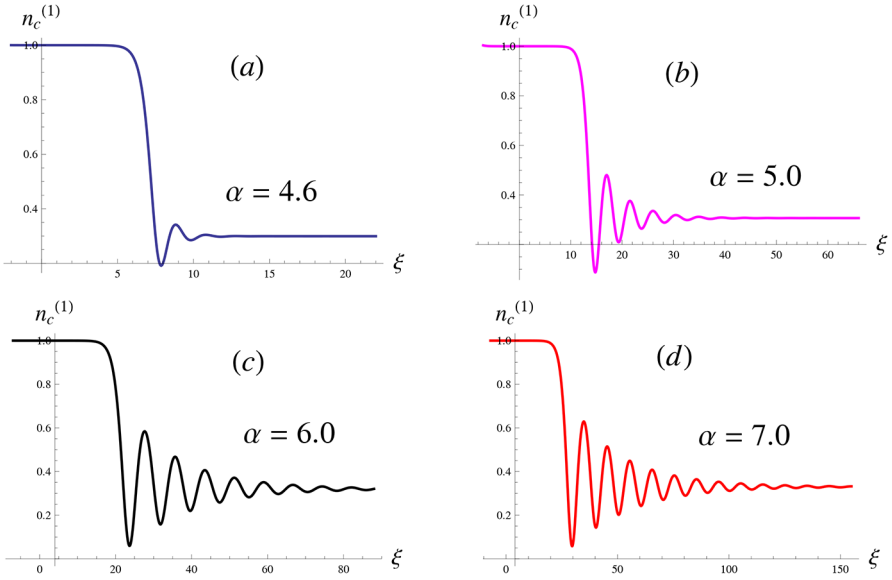

Fig. 4. Plot of $n_c^{(1)}$ for different values of α, for $\eta_0 = 0.04$, $T_F = 1.5 \times 10^8\, K$, $B_0 = 5 \times 10^{10}\, G$, $n_{h0} = 1.1 \times 10^{29}\, \mathrm{cm}^{-3}$ and $l_z = 0.8$.

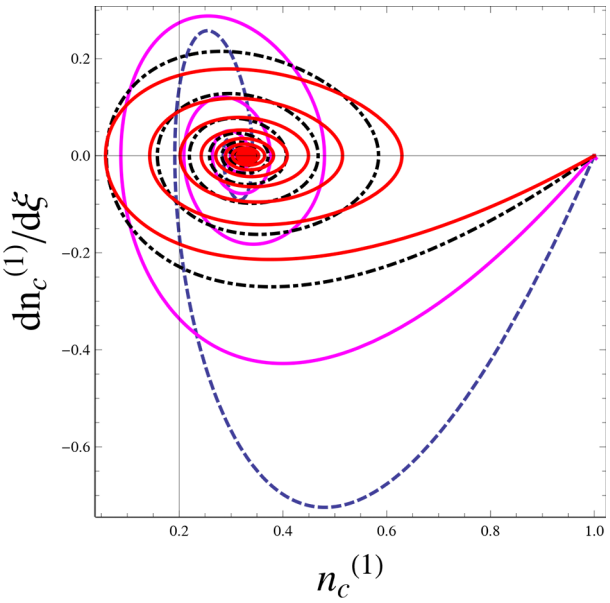

Fig. 5. Plot showing phase portraits $n_c^{(1)}$ *versus* $\mathrm{d}n_c^{(1)}/\mathrm{d}\xi$ for different values of α, for $\eta_0 = 0.04$, $T_F = 1.5 \times 10^8\, K$, $B_0 = 5 \times 10^{10}\, G$, $n_{h0} = 1.1 \times 10^{29}\, \mathrm{cm}^{-3}$ and $l_z = 0.8$.

5 Summary and conclusions

To summarize, in this study we presented both linear and nonlinear analyses of electron acoustic waves, in a dissipative, quantum magnetoplasma, with electrons at two different temperatures, in the background of stationary, neutralizing ions. In contrast to classical plasma, the temperature (Fermi temperature T_F) in quantum plasma is directly related to the electron concentration n. So, hot and cold electrons (symbolized by subscripts h and c) refer to dense and sparse populations, respectively. In the approximation of $T_{Fc} \ll T_{Fh}$ (*i.e.*, $n_c \ll n_h$), and the phase velocity of EAWs in between the Fermi velocities of hot and cold electrons ($v_{Fc} \ll \omega/k \ll v_{Fh}$), Landau damping can be avoided. Additionally, the hot electrons can be treated as inertialess fermions while the cold electrons contribute to the dynamics of the system. Applying the reductive perturbation theory, we restricted our study to a weak dissipative force. The justification for doing so lies in the moderately small amplitudes of these electron acoustic waves. Our aim was to primarily see the effects of the external magnetic field B_0, dissipation η, and the ratio of hot to cold electrons α, on the shape of the nonlinear structures.

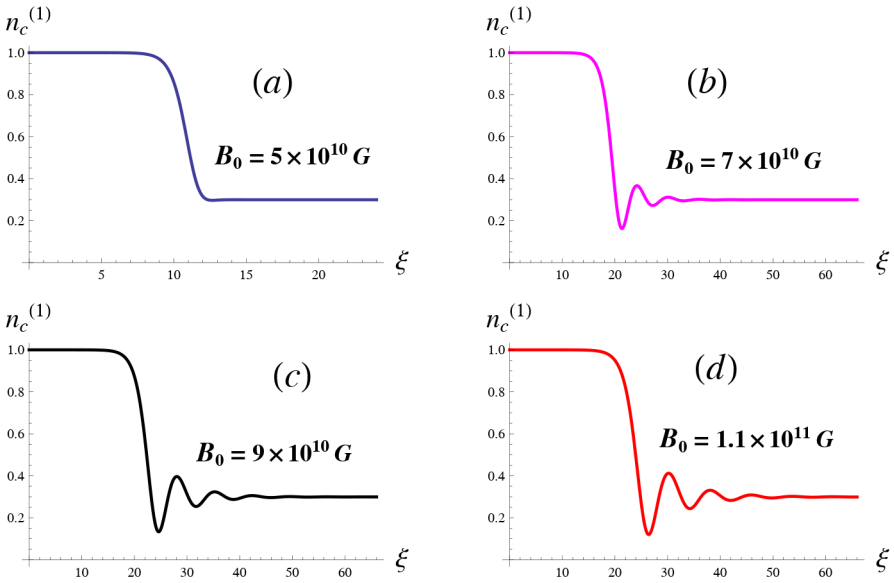

Fig. 6. Plot of $n_c^{(1)}$ for different values of B_0, for $\eta_0 = 0.1$, $T_F = 1.5 \times 10^8\,K$, $\alpha = 4.6$, $n_{h0} = 1.1 \times 10^{29}\,\mathrm{cm}^{-3}$ and $l_z = 0.8$.

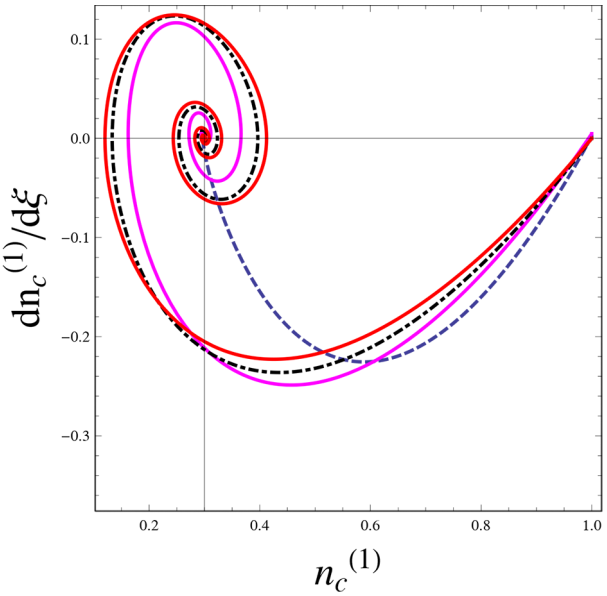

Fig. 7. Plot showing phase portraits $n_c^{(1)}$ *versus* $\mathrm{d}n_c^{(1)}/\mathrm{d}\xi$ for different values of B_0, for $\eta_0 = 0.1$, $T_F = 1.5 \times 10^8\,K$, $\alpha = 4.6$, $n_{h0} = 1.1 \times 10^{29}\,\mathrm{cm}^{-3}$ and $l_z = 0.8$.

The linear analysis yielded a quartic dispersion relation in ω, which imparts an imaginary component to the wave frequency. This produces a decaying wave, with the damping increasing with increasing dissipation. At the same time, the real part of the frequency increases with the fractional decrease in the concentration of cold electrons. These observations were corroborated by graphical plots in fig. 1.

The small amplitude analysis yielded the Korteweg-de Vries-Burgers (KdVB) equation, with the interplay between dissipation and dispersion being determined by the different plasma parameters like η, α and B_0. Interestingly, the absence of any dissipative force renders KdV equation, with soliton solution, whereas strong dissipation gives the Burgers equation with monotonic shock solution. The solutions to the KdVB equation were obtained numerically, using Mathematica. For negligible dissipation, the plot shows a soliton, as expected, whereas for relatively large dissipation, the profile is a monotonic shock. In between, the nonlinear structures are damped oscillations, with the amplitude steadily decreasing with increasing η. These are depicted in fig. 2. On the other hand, the ratio of hot to cold electron concentration has just the opposite effect on the shape of the nonlinear structures —fig. 4. The damping increases (with reduced amplitude) with decrease in the value of α. Additionally, the dispersion is directly related to α. The magnetic field, however, has no impact on the amplitude of the nonlinear waves —fig. 6. A stronger magnetic field only enhances the dispersion of these waves, with increased oscillations. A relatively weaker magnetic field may not support an oscillatory wave, giving a monotonic shock.

We also carried out the stability analysis of the final KdVB equation (31). Of the two critical points obtained, the point $(1, 0)$ is always a saddle point, and hence unstable. The other critical point is a stable focus or a stable node, depending on the relative strengths of the plasma parameters. These findings were endorsed by the phase portrait trajectories plotted in figs. 3, 5 and 7, for varying η, α and B_0, respectively.

To conclude, the results in this study, along with figs. 1 to 7, reveal the following observations:

- the linear dispersion relation gives a complex wave frequency, indicating a decaying wave, with the amount of damping being determined by the dissipation term η;
- the amplitude of the nonlinear waves is affected directly by η, indirectly by α, and not at all by B_0;
- the dispersion gets enhanced by a stronger magnetic field and a higher value of α;
- oscillations prevail for a longer time with increase in B_0;
- the stability analysis yields 2 critical points —an unstable saddle point and an asymptotically stable focus or node, depending on the values of the plasma parameters.

With the existence of such waves in laser produced plasmas, dense astrophysical environment and geomagnetic tail, it is anticipated that our findings in this study might help in understanding certain features of the finite-amplitude localized electron acoustic solitary pulses in a two-population electron Fermi gas. We propose to extend our work to arbitrary amplitude nonlinear structures in the near future.

One of the authors (AS) thanks the Department of Science and Technology, Govt. of India, for financial assistance, through its grant SR/WOS-A/PM-14/2016.

References

1. B.D. Fried, R.W. Gould, Phys. Fluids **4**, 139 (1961).
2. P.K. Shukla, L. Stenflo, M.A. Hellberg, Phys. Rev. E **66**, 027403 (2002).
3. R.L. Tokar, S.P. Gary, Geophys. Res. Lett. **11**, 1180 (1984).
4. V. Singh, G.S. Lakhina, Planet. Space Sci. **49**, 107 (2001).
5. H. Matsumoto, H. Kojima, T. Miyatake, Y. Omura, M. Okada, I. Nagano, M. Tsutsui, Geophys. Res. Lett. **21**, 2915 (1994).
6. D. Schriver, M. Ashour-Abdalla, Geophys. Res. Lett. **16**, 899 (1989).
7. F. Anderegg, C.F. Driscoll, D.H.E. Dubin, T.M. ONeil, F. Valentini, Phys. Plasmas **16**, 055705 (2009).
8. M.A. Hellberg, R.L. Mace, R.J. Armstrong, G. Karlstad, J. Plasma Phys. **64**, 433 (2000).
9. S. Chowdhury, S. Biswas, N. Chakrabarti, R. Pal, Phys. Plasmas **24**, 062111 (2017).
10. H. Chen, S.Q. Liu, Astrophys. Space Sci. **339**, 179 (2012).
11. W. Masood, A. Mushtaq, Phys. Plasmas **15**, 022306 (2008).
12. I. Kourakis, P.K. Shukla, J. Phys. A: Math. Gen. **36**, 11901 (2003).
13. M. Dutta, S. Ghosh, N. Chakrabarti, Phys. Rev. E **86**, 066408 (2012).
14. A. Mannan, A.A. Mamun, Astrophys. Space Sci. **340**, 109 (2012).
15. M. Shalaby, S.K. El-Labany, R. Sabry, L.S. El-Sherif, Phys. Plasmas **18**, 062305 (2011).
16. S.S. Varghese, S.S. Ghosh, Phys. Plasmas **23**, 082304 (2016).
17. P. Chatterjee, R.K. Roychoudhury, J. Plasma Phys. **53**, 25 (1995).
18. M. Berthomier, R. Pottelette, M. Malingre, Y. Khotyaintsev, Phys. Plasmas **7**, 2987 (2000).
19. A.A. Mamun, P.K. Shukla, J. Geophys. Res. **107**, 1135 (2002).
20. R.L. Mace, M.A. Hellberg, Phys. Plasmas **8**, 2649 (2001).
21. A.A. Mamun, P.K. Shukla, L. Stenflo, Phys. Plasmas **9**, 1474 (2002).
22. M. Berthomier, R. Pottelette, L. Muschietti, I. Roth, C.W. Carlson, Geophys. Res. Lett. **30**, 2148 (2003).
23. I. Tasnim, M.M. Masud, M. Asaduzzaman, A.A. Mamun, Chaos **23**, 013147 (2013).
24. M.S. Asam, M.J. Uddin, M.M. Masud, A.A. Mamun, Chaos **24**, 033130 (2014).
25. A. Saha, P. Chatterjee, Eur. Phys. J. Plus **130**, 222 (2015).
26. D. Kremp, Th. Bornath, M. Bonitz, M. Shlanges, Phys. Rev. E **60**, 4725 (1999).
27. A.V. Andreev, JETP Lett. **72**, 238 (2000).
28. R. Bingham, J.T. Mendona, P.K. Shukla, Plasma Phys. Controlled Fusion **46**, R1 (2004).
29. M. Marklund, P.K. Shukla, Rev. Mod. Phys. **78**, 591 (2006).
30. G. Chabier, F. Douchin, Y. Potekhin, J. Phys.: Condens. Matter **14**, 133 (2002).
31. Y.F. Jung, Phys. Plasmas **8**, 3842 (2001).
32. Z. Zhenni, W.U. Zhengwei, L.I. Chunhua, Y. Weihong, Plasma Sci. Technol. **16**, 995 (2014).
33. S. Chandra, S.N. Paul, B. Ghosh, Astrophys. Space Sci. **343**, 231 (2013).
34. A. Atteya, E.E. Behery, W.F. El-Taibany, Eur. Phys. J. Plus **132**, 109 (2017).
35. S.K. El-Labany, E.F. El-Shamy, M.G. El-Mahgoub, Phys. Plasmas **19**, 062105 (2012).
36. F. Haas, S. Mahmood, Phys. Rev. E **94**, 033212 (2016).
37. D.M. Saaduzzaman, A. Amina, A.A. Mamun, J. Phys. Soc. Jpn. **87**, 034502 (2018).

38. H. Washimi, T. Tanuiti, Phys. Rev. Lett. **17**, 996 (1966).
39. W. Masood, A.M. Mirza, M. Hanif, Phys. Plasmas **15**, 072106 (2008).
40. H.R. Pakzad, Astrophys. Space Sci. **331**, 169 (2011).
41. J.-F. Zhang, Y.-Y. Wang, Phys. Plasmas **13**, 022303 (2006).
42. V.I. Karpman, *Nonlinear Waves in Dispersive Media* (Pergamon, London, 1975).
43. W. Masood, B. Eliasson, Phys. Plasmas **18**, 034503 (2011).